The Aiding of a Low-Cost Strapdown Inertial Measurement Unit Using Vehicle Model Constraints for Land Vehicle Applications

Gamini Dissanayake, Salah Sukkarieh, *Associate Member, IEEE*, Eduardo Nebot, *Member, IEEE*, and Hugh Durrant-Whyte

***Abstract*—This paper presents a new method for improving the accuracy of inertial measurement units (IMUs) mounted on land vehicles. In contrast to the typical techniques used for IMUs mounted on flight vehicles, the algorithm exploits nonholonomic constraints that govern the motion of a vehicle on a surface to obtain velocity observation measurements which aid in the estimation of the alignment of the IMU as well as the forward velocity of the vehicle. It is shown that this can be achieved without any external sensing provided that certain observability conditions are met. A theoretical analysis is provided together with a comparison of experimental results between a nonlinear implementation of the algorithm and an IMU/GPS navigation system. This comparison demonstrates the effectiveness of the algorithm. The real time implementation is also addressed through a multiple observation inertial aiding algorithm based on the information filter. The observations used in the information filter include position and velocity of the vehicle from a GPS unit, speed from a wheel encoder, and virtual observations due to the constraints on the motion of the vehicle. The results show that the use of these constraints and vehicle speed guarantees the observability of the velocity and the attitude of the inertial unit, and hence bounds the errors associated with these states. The observations from the GPS unit adds extra information to the estimate of these states as well as providing observability of position. The strategies proposed in this paper provides for a tighter navigation loop which can sustain outages of GPS for a greater amount of time as compared to when the inertial unit is used with standard integration algorithms.**

***Index Terms*—Aiding, inertial measurement units, Kalman filter, vehicle modeling.**

I. Introduction

With the commercial development of autonomous land vehicles in applications such as surface and underground mining [1], [2], agriculture [3], and cargo handling [4], there has been a corresponding development of navigation systems. Such systems are necessary to provide knowledge of vehicle position and trajectory and subsequently to control the vehicle along a desired path. Reliable localization is an essential component of any autonomous vehicle. The basic navigation loop implemented in a typical land vehicle is based on dead reckoning sensors, which predict the vehicle's high frequency maneuvers, and low frequency absolute sensors which bound the positioning errors associated with the high frequency sensors [5].

Wheel and steering encoders are extremely effective dead reckoning sensors in planar environments but do not provide accurate information when the deviation from planar motion is significant [6]. A full six-degree-of-freedom inertial measurement unit (IMU) can provide 3-D position and velocity information. A typical IMU consists of three accelerometers and three gyroscopes mounted in a set of three orthogonal axes. The IMU measures the acceleration and the rotation rate of the vehicle in all three dimensions at a high sampling rate, typically at frequencies higher than 100 Hz. From this information, attitude, velocity and hence position of the vehicle can be derived.

Inertial units have always been presented as a valuable sensor in many applications. The advantages of inertial navigation are well known: high update rates; position and velocity in three dimensions along with attitude and heading information; and with no requirement of a vehicle model. However, until recently the high cost of these units has always kept them from being implemented in civilian applications. The major driving force behind the drop in price has been the development of cheaper gyroscopes, generally in a ceramic version [7], [8], and recently silicon models, [9], [10]. This reduction in cost however, has also led to a drop in accuracy of the inertial unit as a whole. The predominant error sources in the inertial sensors, whether they are gyros or accelerometers, is bias, scale factors and random walk, [11]. It is the errors encountered in the gyros which have the most detrimental affect on the inertial navigation output, since these errors are reflected directly into the computed attitude. Attitude of the IMU is used to compute and cancel the effect of the gravitational acceleration on the observed accelerations. As typical vehicle accelerations are significantly smaller than the gravitational acceleration, even small errors in the attitude, lead to large drifts in the velocity and hence position estimates. Attitude errors due to the biases are usually accounted for by estimation or through temperature compensation, especially since there is a strong correlation between changes in bias and changes in temperature. It is the random walk, due to the mathematical integration of signal noise, which cannot be combated unless external sensors are used to constantly bound the errors.

In military applications, external sensors used for the aiding of inertial units have taken on many forms, doppler radar, global positioning system (GPS) and star trackers to name a few. In the civilian sector GPS is used as the external sensor due to the increasing popularity and decreasing cost of this

Manuscript received August 18, 2000; revised April 17, 2001. This paper was recommended for publication by Associate Editor M. Buehler and Editor S. Hutchinson upon evaluation of the reviewers' comments.

The authors are with the Australian Centre for Field Robotics School of Aerospace, Mechanical and Mechatronic Engineering, The University of Sydney, Sydney, NSW 2006, Australia (e-mail: dissa@acfr.usyd.edu.au; salah@acfr.usyd.edu; nebot@acfr.usyd.edu.au; hugh@acfr.usyd.edu.au).

Publisher Item Identifier S 1042-296X(01)10022-4.

1042–296X/01$10.00 © 2001 IEEE

navigation sensor. Since GPS does not require a vehicle model, the IMU/GPS navigation suite is independent of vehicle kinematics. At the Australian Centre for Field Robotics (ACFR), the GPS aiding of inertial units has been used extensively in many land vehicle applications [11],[12]. This navigation suite has been developed to a level where centimeter accuracy can be attained with low-cost inertial units together with the use of carrier phase-differential GPS. Furthermore, fault-detection techniques have also been incorporated to increase the integrity of the navigation suite, by detecting errors such as multipath of the GPS signal. It is during the periods where the decision analysis detects faults in the GPS signal that the inertial unit is left to perform on its own. The resulting lack of external information causes the navigation output of the inertial unit to drift. The drift rate depends on the accuracy of the IMU and the length of time where there are no external observations. Obviously for autonomous applications the longer the inertial unit can maintain a position estimate that is acceptable for a given practical application, in the absence of external observations, the greater the integrity of the navigation system.

There is a vast body of literature on the strategies for using IMUs for position estimation. These are typically based on algorithms developed for IMUs mounted on flight vehicles. Except in the case of a recent study reported in [13] that discusses the aiding of an IMU using aircraft dynamics, none of these strategies pay attention to the behavior of the vehicle on which the IMU is mounted. Clearly, unlike in an aircraft, there is scope to exploit the fact that land vehicles are constrained to move on a surface. One contribution of this paper is the formulation of the equations governing the behavior of an IMU mounted on a land vehicle. It is shown that the presence of nonholonomic constraints for a vehicle moving on a surface allows for the online estimation of the roll, pitch and the forward velocity of the vehicle from the measurements obtained from the IMU. Results from experiments using an instrumented car and from computer simulations are presented. It is shown that the rate of growth of the error in position estimates obtained from an IMU can be substantially reduced when a vehicle model with constraints is used. This is clearly of value when external information, for example, from GPS, is not available for extended periods of time due to outages in the GPS signal.

An observability analysis is also presented to determine the conditions that guarantee observability of attitude and forward velocity. It is demonstrated with theoretical and experimental results that forward velocity is unobservable when certain degrees of freedom are not excited. This is the case when the vehicle is travelling along a straight path, without any pitching or yawing motion. In such situations the speed of the vehicle needs to be measured, typically achieved with the addition of a wheel encoder. Furthermore, heading and position of the vehicle are always unobservable. Therefore, external information, for example from a GPS is always required if it is necessary to use an IMU for navigation over long periods of time.

Finally, this paper also presents a real time algorithm for the aiding of an inertial unit with the three forms of observations mentioned above, namely position and velocity derived from GPS, speed from a wheel encoder and virtual observations due to the constraints on the motion of the vehicle. The fusion of these observations is achieved using a linear information filter. It is particularly easy to fuse observations at different rates originating from different sensors using an information filter, making it computationally more efficient than the standard Kalman filter implementations. It is shown that the assumptions on linearity are valid for a practical system and that the use of additional sensors significantly improve the quality of the position estimate. This is of fundamental importance since it makes the inertial system less dependent on external information.

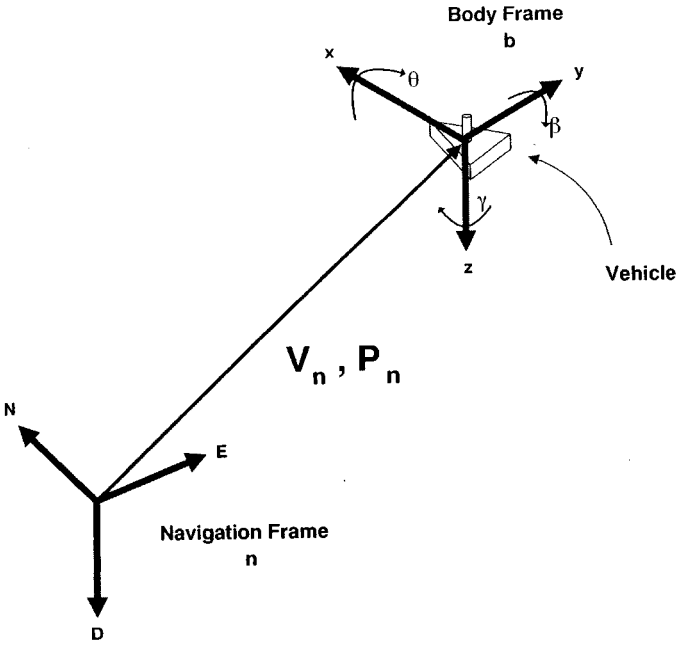

Fig. 1. Motion of a vehicle on a surface. The navigation frame ($\mathbf{n}$) is fixed and is represented by the North, East, and Down axes. The body frame ($\mathbf{b}$) is on the local tangent plane to the surface and is aligned with the kinematic axes of the vehicle. The rotation angles about the x, y and z axes is represented by roll ϕ, pitch θ, and yaw ψ, respectively.

The paper is organized as follows. Section II provides the theoretical background and the observability analysis. Section III presents the information filter implementation. Section IV provides results using simulated and real data and Section V will give the conclusions.

II. Motion of a Land Vehicle

A. General Three-Dimensional (3-D) Motion

Fig. 1 shows a wheeled vehicle moving on the earth surface. The Navigation frame $\mathbf{n}$ represented by the orthogonal axis North, East, and Down (NED) is the coordinate frame with respect to which the location of the vehicle needs to be estimated. The coordinate frame $\mathbf{b}$ is attached to the vehicle and is aligned with the axes of the IMU. Without any loss of generality, assume that the IMU is placed at the center of the rear axle of the vehicle such that $\mathbf{b}_y$ is in the direction of the rear axle and $\mathbf{b}_\mathrm{x}$ is in the direction of forward motion of the vehicle.

It is also assumed that the vehicle is steered using the front wheels. Position of the vehicle $\mathbf{P}_\mathbf{n} = [\mathbf{P}_{nx}, \mathrm{P}_{ny}, \mathrm{P}_{nz}]^\mathrm{T}$ is the position vector of the origin of frame $\mathbf{b}$ in the navigation frame and velocity of the vehicle $\mathbf{V}_\mathbf{n} = [\mathbf{V}_{nx}, \mathbf{V}_{ny}, \mathbf{V}_{nz}]^\mathrm{T}$ is the rate of change of $\mathbf{P}_\mathbf{n}$.

The orientation of the vehicle is represented by the three Euler angles, yaw (ψ), pitch (θ), and roll (ϕ), where the order of rotation is about $\mathbf{b}_z$ followed by $\mathbf{b}_y$ and then $\mathbf{b}_{\mathrm{x}}$. This results in a rotation matrix describing the orientation of frame $\mathbf{b}$ with respect to the navigation frame

$$C_b^n = \begin{bmatrix} \theta_c\psi_c & -\phi_c\psi_s + \phi_s\theta_s\psi_c & \phi_s\psi_s + \phi_c\theta_s\psi_c \\ \theta_c\psi_s & \phi_c\psi_c + \phi_s\theta_s\psi_s & -\phi_s\psi_c + \phi_c\theta_s\psi_s \\ -\theta_s & \phi_s\theta_c & \phi_c\theta_c \end{bmatrix}$$

where the subscripts s and c refer to sine and cosine. Measurements of the IMU are the accelerations $\mathbf{A}_b = [\mathbf{A}_{bx}, \mathbf{A}_{by}, \mathbf{A}_{bz}]^{\mathrm{T}}$ and angular velocities $\boldsymbol{\omega}_b = [\omega_{bx}, \omega_{by}, \omega_{bz}]^{\mathrm{T}}$ in the body frame $\mathbf{b}$. Let the motion of the vehicle be described by the state equation

$$\dot{\mathbf{x}} = \mathbf{f}(\mathbf{x}, \mathbf{u}) \tag{1}$$

where the vehicle state vector $\mathbf{x} = \left[\mathbf{P}_{\mathbf{n}}^{\mathrm{T}}, \mathbf{V}_{\mathbf{n}}^{\mathrm{T}}, \psi, \theta, \phi\right]^{\mathrm{T}}$, and the measurements $\mathbf{u} = \left[\mathbf{A}_b^{\mathrm{T}}, \boldsymbol{\omega}_b^{\mathrm{T}}\right]^{\mathrm{T}}$.

Assuming that, in the context of a land vehicle, the gravity vector $\mathbf{G}$ is constant parallel to $\mathbf{n}_z$, the accelerations measured by the IMU are related to the accelerations in the navigation frame $\mathbf{A}_{\mathrm{n}}$ by

$$\mathbf{A}_b = \left[\mathbf{C}_b^n\right]^{\mathrm{T}} \left[\mathbf{A}_{\mathrm{n}} + \mathbf{G}\right]. \tag{2}$$

Equation (2) was derived using the orthogonal properties of $\mathbf{C}_b^n$ where the inverse of this matrix is simply its transpose.

Using the kinematic relationship between $\boldsymbol{\omega}_b$ and the rates of changes of the Euler angles, and assuming that the rate of rotation of the earth is negligible, the state equations for vehicle motion can now be written as

$$\dot{\mathbf{P}}_{\mathbf{n}} = \mathbf{V}_{\mathbf{n}} \tag{3}$$

$$\dot{\mathbf{V}}_{\mathbf{n}} = \mathbf{C}_b^n \mathbf{A}_b - \mathbf{G} \tag{4}$$

$$\dot{\psi} = \frac{\omega_{by}\sin\phi + \omega_{bz}\cos\phi}{\cos\theta} \tag{5}$$

$$\dot{\theta} = \omega_{by}\cos\phi - \omega_{bz}\sin\phi \tag{6}$$

$$\dot{\phi} = \omega_{bx} + (\omega_{by}\sin\phi + \omega_{bz}\cos\phi)\tan\theta. \tag{7}$$

Equations (3)–(7) are the fundamental equations that enable the computation of the state $\mathbf{x}$ of the vehicle from an initial state $\mathbf{x}(0)$ and a series of measurements $\mathbf{A}_b$ and $\boldsymbol{\omega}_b$. It is important to note the following with respect to these equations.

1) These equations are valid for the general motion of a body in three-dimensional space. It should be pointed out that in some inertial applications, effects such as the Schuler frequency, Earth rotation, and the fact that gravity is not necessarily constant as the vehicle traverses over large distances, modifies the equation stated here. However, for low cost IMU's which cannot measure such effect, or changes in these effects, these terms do not find their way into these equations. This is coupled to the fact that in many land, civilian applications, as concerned with in this paper, the error drift in the INS solutions is dramatic enough to warrant constant aiding.
2) Equations (4)–(7) represent a set of nonlinear differential equations that can easily be solved using a variety of different techniques. If the sampling time is sufficiently small, as usually is the case in many practical applications, a simple Euler scheme is adequate.
3) It is possible to linearize these equations, for sufficiently small sampling intervals, by incorporating all the elements of the direction cosine matrix $\mathbf{C}_b^n$ into the state equation. Although this approach ignores the intrinsic relationship between the elements of $\mathbf{C}_b^n$ practical experience suggests that this is not an important issue and the computational efficiency gained is substantial. Alternative schemes for representing orientation of a body can also be used, eg. quaternions, in the formulation of state equations.
4) When $\theta = \pm\pi/2$, the set of equations presented above is singular. Although this is important for airborne vehicles, this condition is equivalent to driving up or down a 90 degree slope, therefore, will not occur in the case of land vehicles.
5) Two factors contribute to the rapid growth in the error of position estimates computed using measurements of a typical IMU.
   a) The estimate for the vehicle position $\mathbf{P}_{\mathbf{n}}$ is arrived at after three integration steps in time t. One integration to obtain the Euler angles θ and ϕ from measured $\boldsymbol{\omega}_b$; then compute $\mathbf{A}_{\mathbf{n}}$ using measured $\mathbf{A}_b$, θ and ϕ; integrate $\mathbf{A}_{\mathbf{n}}$ twice to obtain $\mathbf{P}_{\mathbf{n}}$. The error in the position estimate due to any unidentified bias in the gyroscopes will, therefore, be proportional to t^3. In addition, any Gaussian noise present in the IMU readings will deliver a drifting INS solution of random walk (Brownian Motion) behavior, which can be characterized as an error proportional to $\sqrt{t}$ as demonstrated in [11], after each integration step.
   b) Typical accelerations $\mathbf{A}_{\mathbf{n}}$ for land vehicles are small compared to the gravity vector $\mathbf{G}$. Therefore, even small errors in the estimated attitude of the vehicle, hence $\mathbf{C}_b^n$, can introduce large errors in the computed vehicle acceleration.

Clearly, the rate of error growth can be reduced if the velocity of the vehicle and the Euler angles θ and ϕ can be estimated directly. It will be shown in the next section that this is indeed possible for a vehicle moving on a surface by exploiting the resulting nonholonomic constraints.

B. Motion of a Vehicle on a Surface

Unlike in the case of a flight vehicle, motion of a wheeled vehicle on a surface is governed by two nonholonomic constraints. When the vehicle does not jump off the ground and does not slide on the ground, velocity of the vehicle in the plane perpendicular to the forward direction is zero. Under ideal conditions, there is no side slip along the direction of the rear axle and no motion normal to the road surface, the constraints are

$$V_{by} = 0 \tag{8}$$

$$V_{bz} = 0. \tag{9}$$

In any practical situation, these constraints are somewhat violated due to the presence of side slip during cornering and vibrations caused by the engine and suspension system. In partic-

ular the side slip is a function of the vehicle state as well as the interaction between the vehicle tyres and the terrain.

A number of models are available for determining side slip, but these models require the knowledge of the vehicle, tyre and ground characteristics that are not generally available. Alternatively, information from external sensors can be used to estimate slip on-line. As a first approximation, however, it is possible to model the extent of constraint violations as follows:

$$V_{by} - \nu_y = 0 \tag{10}$$

$$V_{bz} - \nu_z = 0 \tag{11}$$

where ν_y and ν_z are Gaussian white noise sources with zero mean and variance σ_y^2 and σ_z^2, respectively. The strength of the noise can be chosen to reflect the extent of the expected constraint violations.

Using the following equation that relates the velocities in the body frame $\mathbf{V}_b = [V_{bx}, V_{by}, V_{bz}]^{\mathrm{T}}$ to $\mathbf{V}_{\mathbf{n}}$:

$$\mathbf{V}_b = [\mathbf{C}_b^n]^{\mathrm{T}} \mathbf{V}_{\mathbf{n}}$$

it is possible to write constraint (10) and (11) as a function of the vehicle state $\mathbf{x}$ and a noise vector $\mathbf{w} = [\nu_y, \nu_z]^{\mathrm{T}}$

$$\begin{bmatrix} V_{by} \\ V_{bz} \end{bmatrix} = \mathbf{M} + \begin{bmatrix} \nu_y \\ \nu_z \end{bmatrix} \tag{12}$$

where $\mathbf{M}$ is given in (13), shown at bottom of the page. It is now required to obtain the best estimate for the state vector $\mathbf{x}$ modeled by the state (4)–(7) from a series of measurements $\mathbf{A}_b$ and $\boldsymbol{\omega}_b$, subjected to the constraint (12). An estimation theoretic approach based on the extended Kalman filter for this purpose is described in the following subsection.

C. Estimation of the Vehicle State in the Presence of Constraints

The state equation, obtained by the discretization (4)–(7), is

$$\mathbf{x}(k) = \mathbf{f}(\mathbf{x}(k-1), \mathbf{u}(k-1), (k-1) \tag{14}$$

and the discrete time version of the constraint equation obtained from (12)

$$\mathbf{z}(k) = \mathbf{h}(\mathbf{x}(k), \mathbf{w}(k)) \tag{15}$$

where k is the time step and $\mathbf{z}(\mathbf{k})$ is expected to be zero.

Estimation of the state vector $\mathbf{x}$ subjected to stochastic constraints can be done in the framework of an extended Kalman filter.

It is proposed to treat (15) as an observation equation where the "virtual observation" at each time instant k is in fact identical to zero. The Kalman filter recursively computes estimates for a state $\mathbf{x}(\mathbf{k})$ which is evolving according to the process model in (14) and which is being observed according to the observation model in (15). The filter computes an estimate which is equivalent to the conditional mean $\hat{\mathrm{x}}(\mathbf{p}|\mathbf{q}) = \mathbf{E}[\mathbf{x}(\mathbf{p})|\mathbf{Z}^{\mathrm{q}}](p \geq q)$, where $\mathbf{Z}^{\mathrm{q}}$ is the sequence of observations taken up to time q, are all equal to zero. The error in the estimate is denoted $\tilde{\mathrm{x}}(\mathbf{p}|\mathbf{q}) = \hat{\mathrm{x}}(\mathbf{p}|\mathbf{q}) - \mathbf{x}(\mathbf{p})$. The Kalman filter also provides a recursive estimate of the covariance $\mathbf{P}(\mathbf{p}|\mathbf{q}) = \mathbf{E}\left[\tilde{\mathrm{x}}(\mathbf{p}|\mathbf{q})\tilde{\mathrm{x}}(\mathbf{p}|\mathbf{q})^{\mathrm{T}}|\mathbf{Z}^{\mathrm{q}}\right]$ in the estimate $\hat{\mathrm{x}}(\mathbf{p}|\mathbf{q})$. We briefly summarize the algorithm here for completeness. Detailed descriptions may be found in [14].The Kalman filter algorithm proceeds recursively in three stages.

Prediction: Given that the models described in (14) and (15) hold, and that an estimate $\hat{\mathrm{x}}(\mathbf{k}|\mathbf{k})$ of the state $\mathbf{x}(\mathbf{k})$ at time k together with an estimate of the covariance $\mathbf{P}(\mathbf{k}|\mathbf{k})$ exist, the algorithm first generates a prediction for the state estimate, the observation and the state estimate covariance at time $k+1$ according to

$$\hat{\mathbf{x}}(k|k-1) = \mathbf{f}(\hat{\mathbf{x}}(k-1|k-1), \mathbf{u}(k-1), (k-1) \tag{16}$$

$$\hat{\mathbf{z}}(k|k-1) = \mathbf{h}(k-1)\hat{\mathbf{x}}(k|k-1) \tag{17}$$

$$\begin{aligned}\mathbf{P}(k|k-1) = {} & \nabla \mathbf{f}_x(k-1)\mathbf{P}(k-1|k-1)\nabla \mathbf{f}_x(k-1)^T \\ & + \nabla \mathbf{f}_u(k-1)\mathbf{Q}\nabla \mathbf{f}_u(k-1)^T\end{aligned} \tag{18}$$

respectively.

Observation: Following the prediction, it is assumed that an observation $\mathbf{z}(k)$ that is identical to zero is made. An innovation is then calculated as follows:

$$\boldsymbol{\nu}(k) = \mathbf{z}(k) - \hat{\mathbf{z}}(k|k-1) \tag{19}$$

where $\mathbf{z}(k)$ is in fact set to zero. An associated innovation covariance given by the following equation is also computed:

$$\begin{aligned}\mathbf{S}(k|k-1) = {} & \nabla \mathbf{h}_x(k-1)\mathbf{P}(k|k-1)\nabla \mathbf{h}_x(k-1)^T \\ & + \nabla \mathbf{h}_w(k-1)\mathbf{R}(k-1)\nabla \mathbf{h}_w(k-1)^T\end{aligned} \tag{20}$$

Update: The state estimate and corresponding state estimate covariance are then updated according to

$$\hat{\mathbf{x}}(k|k) = \hat{\mathbf{x}}(k|k-1) + \mathbf{W}(k)(\mathbf{z}(k) - \mathbf{h}(\hat{\mathbf{x}}(k|k-1)))$$

$$\mathbf{P}(k|k) = \mathbf{P}(k|k-1) - \mathbf{W}(k)\mathbf{S}(k)\mathbf{W}^T(k)$$

where the gain matrix $\mathbf{W}(\mathbf{k}+\mathbf{1})$ is given by

$$\mathbf{W}(k) = \mathbf{P}(k|k-1)\nabla \mathbf{h}_x(k-1)^T \mathbf{S}^{-1}(k) \tag{21}$$

where ∇ represents the gradient operator, and $\mathbf{Q}$ and $\mathbf{R}$ are matrices representing noise in the IMU measurements and the constraint equations, respectively.

D. Observability of the States

Although an extended Kalman filter algorithm was developed in the previous section in order to obtain estimates of the state $\mathbf{x}$, not all the state variables are observable. For example, inspection of the state equation; the position, velocity and attitude vector, and

$$\begin{bmatrix} V_{nx}\cos\theta\cos\psi + V_{ny}\cos\theta\sin\psi - V_{nz}\sin\theta \\ V_{nx}(\sin\phi\sin\theta\cos\psi - \cos\phi\sin\psi) + V_{ny}(\cos\phi\cos\psi + \sin\phi\sin\theta\sin\psi) + V_{nz}\sin\phi\cos \end{bmatrix} \tag{13}$$

observation equation; velocity measurements along the normal and axial directions, suggest that the estimation of the vehicle position, $\mathbf{P_n}$, requires direct integrations and therefore is not observable. Furthermore, if the vehicle moves in a trajectory that does not excite the relevant degrees-of-freedom, the number of observable states may be further reduced. Intuitively, forward velocity is the direct integral of the measured forward acceleration during motion along straight lines, therefore is not observable. Clearly an analysis is required to establish the conditions of observability. As the state and observation equations are nonlinear, this is not straightforward. In this section an alternative formulation of the state equations, that directly incorporates the nonholonomic constrains, are developed in order to examine this issue.

Consider the motion of a vehicle on a surface as shown in Fig. 1. Assume that the nonholonomic constraints are strictly enforced and therefore the velocity vector of the vehicle in the navigation frame $\mathbf{V_n}$ is aligned with $\mathbf{b_x}$. Let $s, \dot{s}$ and $\ddot{s}$ be the distance measured from some reference location to the current vehicle location along its path, and its first and second derivatives with respect to time. Therefore

$$\mathbf{V} = \dot{s}\mathbf{b_x}$$

Acceleration of the vehicle is given by

$$\mathbf{A} = \dot{\mathbf{V}} = \ddot{s}\mathbf{b_x} + \dot{s}\dot{\mathbf{b}}_\mathbf{x}.$$

As the angular velocity of the coordinate frame $\mathbf{B}$ is given by $\boldsymbol{\omega}_b$, then

$$\mathbf{A} = \ddot{s}\mathbf{b_x} + \dot{s}\boldsymbol{\omega_b} \times \mathbf{b_x}$$
$$\mathbf{A} = \ddot{s}\mathbf{b_x} + \dot{s}\omega_z\mathbf{b}_y - \dot{s}\omega_y\mathbf{b}_z.$$

Components of the acceleration of the vehicle in the body frame $\mathbf{B}$ become

$$\mathbf{A}.\mathbf{b_x} = \ddot{s}$$
$$\mathbf{A}.\mathbf{b}_y = \dot{s}\omega_z$$
$$\mathbf{A}.\mathbf{b}_z = -\dot{s}\omega_y.$$

Using (2) in the above, we obtain

$$\begin{bmatrix} A_{bx} \\ A_{by} \\ A_{bz} \end{bmatrix} = \begin{bmatrix} \dot{V}_f \\ V_f\omega_z \\ -V_f\omega_y \end{bmatrix} + \begin{bmatrix} \theta_c\psi_c & \theta_c\psi_s & -\theta_s \\ -\phi_c\psi_s + \phi_s\theta_s\psi_c & \phi_c\psi_c + \phi_s\theta_s\psi_s & \phi_s\theta_c \\ \phi_s\psi_s + \phi_c\theta_s\psi_c & -\phi_s\psi_c + \phi_c\theta_s\psi_s & \phi_c\theta_c \end{bmatrix} \cdot \begin{bmatrix} 0 \\ 0 \\ -g \end{bmatrix}$$

where g is the gravitational constant and $V_f = \dot{s}$ is the speed of the vehicle. Rearranging the above, the following three equations relating the vehicle motion to the measurements from the IMU can now be obtained:

$$\dot{V}_f - A_{bx} + g\sin\theta = 0 \tag{22}$$
$$V_f\omega_z - A_{by} - g\sin\phi\cos\theta = 0 \tag{23}$$
$$V_f\omega_y + A_{bz} + g\cos\phi\cos\theta = 0. \tag{24}$$

The following points are clear from the above equations.

- When the forward acceleration is zero the roll (ϕ) and pitch (θ) can be directly computed from the IMU measurements.
- If one of the angular velocities ω_y or ω_z is not zero, the forward velocity can also be computed directly.
- Even when the forward acceleration is nonzero, it is possible to write a differential equation containing only the forward velocity and the IMU measurements by substituting (23) and (24) into (22). Therefore, V_f can be obtained by one integration step involving the IMU measurements. If the constraints are not used, two integration steps are required to obtain velocities. This result is of significant importance. The fact that the forward acceleration is observable makes the forward velocity error growth only a function of the random walk due to the noise present in the observed acceleration.
- It is possible to use (23) and (24) directly to obtain the complete vehicle state without going through the Kalman filter proposed in the previous section. This, however, makes it difficult to incorporate models for constraint violations in the solution. Also, when the constraint violation is significant, such as in off road situations or cornering at high speeds, the white noise model is inadequate. For example, if there is significant side slip, explicit slip modeling may be required.

III. The Linear Information Filter Approach

The information filter (IF) is mathematically equivalent to the Kalman filter (KF) and hence produces exactly the same result. The difference between the two is that the IF is developed in information space instead of state space. The distinct advantage of the implementation of the IF is the ease with which one can introduce multiple observations from various sources without the concern of correlations feeding their way through the innovation sequence, as is common with the multiple observation form of the KF. The reader is referred to [15], [16] for the IF derivation and its appeal to multiple sensor applications.

The primary reason for the implementation of the IF in this work is the relative ease of fusing multiple observations from various sensors: position and velocity from GPS, speed from a wheel encoder, and velocity from the nonholonomic constraints previously discussed. The filter also results in a computationally efficient algorithm that is easy to implement in a real time system. As discussed previously, the use of multiple observations provide more accurate state estimates as well as guarantees the observability of position, which is essential in a practical application.

The key components in the IF are the information state matrix, $\mathbf{Y}$, and the information state vector, $\mathbf{y}$. $\mathbf{Y}$ is the inverse of the covariance matrix found in statistical estimation, that is,

$$\mathbf{Y(k)} = \mathbf{P^{-1}(k)} \tag{25}$$

while the information state vector is

$$\mathbf{y(k)} = \mathbf{Y(k)x(k)} \tag{26}$$

where $\mathbf{x(k)}$ is the state vector at time k. The predicted information state vector is given by

$$\mathbf{\tilde{y}(k|k-1)} = \mathbf{\hat{Y}(k|k-1)F(k)\hat{Y}^{-1}(k|k-1)}. \tag{27}$$

The corresponding information state matrix is

$$\tilde{\mathbf{Y}}(\mathbf{k}|\mathbf{k-1}) = [\mathbf{F}(\mathbf{k})\tilde{\mathbf{Y}}^{-1}(\mathbf{k-1}|\mathbf{k-1})\mathbf{F}^{\mathrm{T}}(\mathbf{k}) + \mathbf{Q}(\mathbf{k})]^{-1}$$

where $\mathbf{Q}(\mathbf{k})$ is the process noise of the model $\mathbf{F}(\mathbf{k})$. The model that is implemented in the filter is the standard linear inertial error model employed in typical inertial feedback systems [11],[12]

$$\begin{bmatrix} \boldsymbol{\delta}\dot{\mathbf{p}}_{\mathbf{n}} \\ \boldsymbol{\delta}\dot{\mathbf{v}}_{\mathbf{n}} \\ \boldsymbol{\delta}\dot{\boldsymbol{\psi}}_{\mathbf{n}} \end{bmatrix} = \begin{bmatrix} 0 & \mathbf{I} & 0 \\ 0 & 0 & \mathbf{A}_{\mathbf{n}} \\ 0 & 0 & 0 \end{bmatrix} \begin{bmatrix} \boldsymbol{\delta}\mathbf{p}_{\mathbf{n}} \\ \boldsymbol{\delta}\mathbf{v}_{\mathbf{n}} \\ \boldsymbol{\delta}\boldsymbol{\psi}_{\mathbf{n}} \end{bmatrix}. \tag{28}$$

With this model, the position errors $\boldsymbol{\delta}\dot{\mathbf{p}}_{\mathbf{n}}$, velocity errors $\boldsymbol{\delta}\dot{\mathbf{v}}_{\mathbf{n}}$, and attitude errors $\boldsymbol{\delta}\dot{\boldsymbol{\psi}}_{\mathbf{n}}$, of the inertial navigation system are evaluated during motion. The term $\mathbf{A}_{\mathbf{n}}$, is the acceleration as evaluated by the inertial unit in the navigation frame. The estimated errors are fed back to the inertial navigation solution in order to correct it. This model is an error form of the inertial navigation equations described in (3)–(7). The derivation of this model follows a simple perturbation analysis as outlined in [17].

When an observation $\mathbf{z}(\mathbf{k})$ is made, the information observation vector and the corresponding information observation matrix is formed as

$$\mathbf{i}(\mathbf{k}) = \mathbf{H}^{\mathrm{T}}(\mathbf{k})\mathbf{R}^{-1}(\mathbf{k})\mathbf{z}(\mathbf{k}) \tag{29}$$

$$\mathbf{I}(\mathbf{k}) = \mathbf{H}^{\mathrm{T}}(\mathbf{k})\mathbf{R}^{-1}(\mathbf{k})\mathbf{H}(\mathbf{k}) \tag{30}$$

where $\mathbf{H}(\mathbf{k})$ is the observation model and $\mathbf{R}(\mathbf{k})$ is the observation noise matrix. $\mathbf{i}(\mathbf{k})$ is the information contribution of the observation, $\mathbf{z}(\mathbf{k})$, to the state variables. $\mathbf{I}(\mathbf{k})$ represents the certainty, that is, the amount of information in the observation projected onto the state variables. Once the observations are obtained, the estimate proceeds as

$$\hat{\mathbf{y}}(\mathbf{k}|\mathbf{k}) = \tilde{\mathbf{y}}(\mathbf{k}|\mathbf{k-1}) + \mathbf{i}(\mathbf{k}) \tag{31}$$

$$\tilde{\mathbf{Y}}(\mathbf{k}|\mathbf{k}) = \hat{\mathbf{Y}}(\mathbf{k}|\mathbf{k-1}) + \mathbf{I}(\mathbf{k}) \tag{32}$$

The information observation vector and matrix are generated for any observation from any sensor or a virtual observation generated by the constraints. The benefits of (31) and (32) is that the estimates can be easily computed when multiple aiding is used since the information observation vector and matrix is simply the sum of the individual observation information vectors and matrices, that is,

$$\hat{\mathbf{y}}(\mathbf{k}|\mathbf{k}) = \tilde{\mathbf{y}}(\mathbf{k}|\mathbf{k-1}) + \sum \mathbf{i}_{\mathbf{obs}}(\mathbf{k}) \tag{33}$$

$$\hat{\mathbf{Y}}(\mathbf{k}|\mathbf{k}) = \tilde{\mathbf{Y}}(\mathbf{k}|\mathbf{k-1}) + \sum \mathbf{I}_{\mathbf{obs}}(\mathbf{k}). \tag{34}$$

A. Observations

When an observation from the aiding sensor is made, the observation vector generated is the observed error of the inertial system, that is,

$$\mathbf{z}(\mathbf{k}) = \mathbf{Inertial}_{\mathbf{state}}(\mathbf{k}) - \mathbf{Observation}_{\mathbf{state}}(\mathbf{k}). \tag{35}$$

Once the observation is made, the information state vector is generated along with the corresponding information matrix, (31) and (32), and the estimate proceeds using (33) and (34).

Constraints and the Vehicle Speed: As discussed in Section II-B, motion of the land vehicle is subjected to constraints. Thus, the observation constraints ($Cons_{Vel}$) are

$$Cons_{Vel_y} = 0$$
$$Cons_{Vel_z} = 0.$$

The noise strength is depicted by the observation noise matrix $\mathbf{R}_{\mathrm{cons}}$. At this stage, the velocity vector is only partly completed, requiring the speed of the vehicle in the x direction which is obtained from the speed encoder. The velocity vector that is formed by combining the speed data along with the modeling constraints is termed the "constraint" observation. This observation vector which is in the body frame is converted to the navigation frame using $\mathbf{C}_{\mathbf{b}}^{\mathbf{n}}$. Thus, the observation is

$$\mathbf{z}_{\mathbf{virtual}}(\mathbf{k}) = \mathbf{Inertial}_{\mathbf{Vel}}(\mathbf{k}) - \mathbf{Virtual}_{\mathbf{Vel}}(\mathbf{k}) \tag{36}$$

where

$$\mathbf{Virtual}_{\mathbf{Vel}}(\mathbf{k}) = \mathbf{C}_{\mathbf{b}}^{\mathbf{n}} \begin{pmatrix} \mathrm{Encoder}_{\mathrm{Vel}}(\mathrm{k}) \\ 0 \\ 0 \end{pmatrix}. \tag{37}$$

The observation model is given by

$$\mathbf{H}_{\mathbf{Virtual}}(\mathbf{k}) = (\,\mathbf{0}_{3\times3} \quad \mathbf{I}_{3\times3} \quad \mathbf{0}_{3\times3}\,). \tag{38}$$

The observation covariance matrix is

$$\mathbf{R}_{\mathbf{Virtual}}(\mathbf{k}) = \begin{pmatrix} R_{\mathrm{Encoder_{vel}}}(k) & 0 & 0 \\ 0 & R_{Cons_{Vel_y}}(k) & 0 \\ 0 & 0 & R_{Cons_{Vel_z}}(k) \end{pmatrix}. \tag{39}$$

Since the velocity vector is transformed from the body frame to the navigation frame, the observation noise covariance needs to be transformed as well and is done so by

$$\bar{\mathbf{R}}_{\mathbf{virtual}}(\mathbf{k}) = \mathbf{C}_{\mathbf{b}}^{\mathbf{n}}(\mathbf{k})\, \mathbf{R}_{\mathbf{Virtual}}(\mathbf{k})\, (\mathbf{C}_{\mathbf{b}}^{\mathbf{n}})^{\mathrm{T}}(\mathbf{k}). \tag{40}$$

GPS: When position and velocity are obtained from the GPS, the observation vector is

$$\mathbf{z}_{\mathbf{GPS}}(\mathbf{k}) = \begin{pmatrix} \mathbf{Inertial}_{\mathbf{Pos}}(\mathbf{k}) - \mathbf{GPS}_{\mathbf{Pos}}(\mathbf{k}) \\ \mathbf{Inertial}_{\mathbf{Vel}}(\mathbf{k}) - \mathbf{GPS}_{\mathbf{Vel}}(\mathbf{k}) \end{pmatrix} \tag{41}$$

The GPS observations are obtained in the NED frame. The observation model is

$$\mathbf{H}_{\mathbf{GPS}}(\mathbf{k}) = \begin{pmatrix} \mathbf{I}_{\mathbf{3\times3}} & \mathbf{0}_{\mathbf{3\times3}} & \mathbf{0}_{\mathbf{3\times3}} \\ \mathbf{0}_{\mathbf{3\times3}} & \mathbf{I}_{\mathbf{3\times3}} & \mathbf{0}_{\mathbf{3\times3}} \end{pmatrix}. \tag{42}$$

The observation noise matrix is

$$\mathbf{R}_{\mathbf{GPS}}(\mathbf{k}) = \begin{pmatrix} \mathbf{Pos}_{\mathbf{3\times3}}(\mathbf{k}) & \mathbf{0}_{\mathbf{3\times3}} \\ \mathbf{0}_{\mathbf{3\times3}} & \mathbf{Vel}_{\mathbf{3\times3}}(\mathbf{k}) \end{pmatrix}. \tag{43}$$

IV. Results

This section presents the results of both the computer simulations and experiments on a land vehicle. The simulations are primarily aimed at examining the issues related to the observability of the states when using the algorithm based on constraints described in Section II. The experiments address two areas: IMU without any external observations to demonstrate the use of the

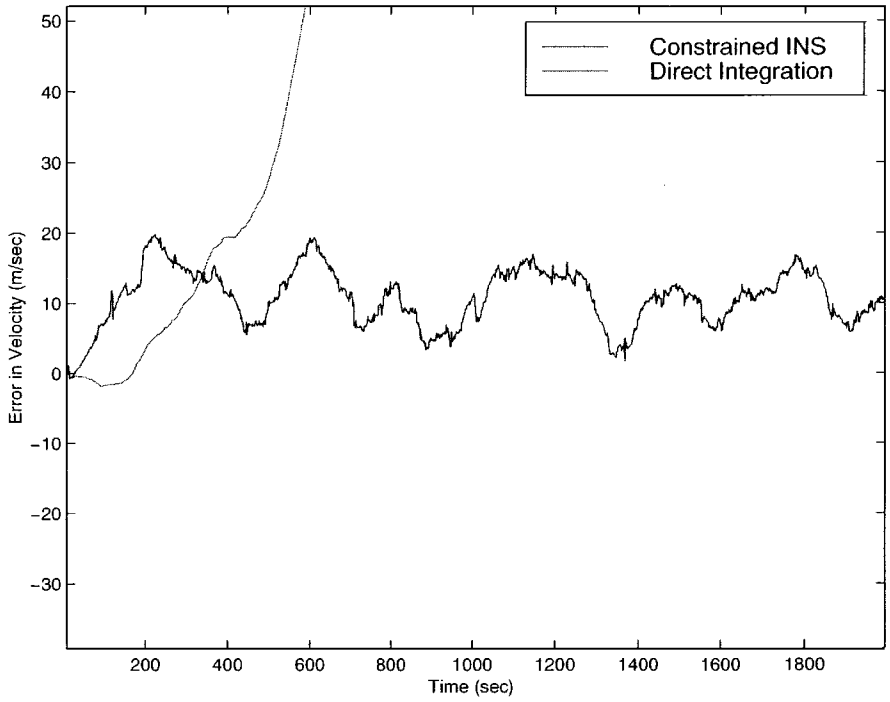

Fig. 2. Errors in vehicle speed when the vehicle is moving at a constant velocity of 10 m/s while the angular velocity about $\mathbf{b}_x$ is nonzero in the time interval 700–1300 s.

algorithm presented in Section II and IMU aided by a vehicle speed sensor and GPS to demonstrate the effectiveness of this algorithm and its implementation through the information filter in a practical land vehicle navigation system.

The test vehicle used in the experimental work, shown in Fig. 8, is a standard utility fitted with the following.

- Ashtech Carrier Phase Differential GPS receivers (GG24) — Rated accuracy of 0.02 m in position and 0.02 m/s in velocity when at least six satellites are in view. Sample rate is 10 *Hz*.
- Watson Inertial Measurement Unit (IMU-BA604) comprising of three VSG's gyros and three Piezo Accelerometers. Sample rate is 125 Hz and provides predicted position, velocity and attitude information after inertial integration.
- Wheel encoder providing forward speed with an accuracy of 1 m/s at 20 Hz. The encoder was mounted on the left back wheel. The resolution of the encoder is 4095 pulses per revolution. Since the wheel encoder provides data at 20 Hz, the constraints can also be applied at this rate since they form one velocity vector (37). However, 20 Hz is fast enough to assume constant velocity between samples, and so the virtual velocity vector can be generated at the same sampling rate as the inertial unit, that is at 125 Hz.

A. Simulation Results

In order to examine the effectiveness and the theoretical limitations of the proposed algorithm, computer simulations were performed where the trial conditions can be accurately controlled. In particular, the effect of not having sufficient excitation that make the algorithm unobservable were examined to verify the predictions made in Section II-D. A program was written to simulate the motion of a wheeled vehicle on a predefined trajectory and generate the resulting accelerations and angular velocities. These accelerations and velocities, corrupted with noise, were then used to generate estimates of the vehicle position and velocity.

To examine the effect of the angular velocities in $\mathbf{b}_x$, $\mathbf{b}_y$, and $\mathbf{b}_z$ on the estimation algorithm, simulated data corresponding to a vehicle moving at constant velocity was generated.

All angular velocities of the vehicle were set to zero except one of the angular velocities was set to a random walk in the time interval between 700 to 1300 s. Figs. 2–4 show the error in the predicted speed of the vehicle V_f. It is seen from these figures, as expected, that any excitation due to ω_{by} and ω_{bz} results in a zero error in predicted vehicle speed where as motion in ω_{bx} has no effect on this error.

It is also seen from Fig. 5 that the errors in roll and pitch do not grow when the proposed algorithm was used for their prediction. This is an important result because as can be seen from Fig. 2, that although the error in velocity is not reduced to zero it only grows due to noise as random walk. Again, as expected, the error in yaw grows with time. This effect is clearer when there are unestimated biases present in the gyroscope readings (see Fig. 6).

Fig. 7 shows that the error in the predicted speed of the vehicle reduces to zero even when the velocity of the vehicle is not constant.

B. Experimental Results With an Unaided IMU

The trial area used in this experiment was a tarred road with gently sloping terrain with an approximate change in elevation of about 6 m. This area was selected so that multipath errors in the GPS were not present. The vehicle was driven at speeds of up to 10 m/s. Fig. 9 shows the position of the vehicle in two

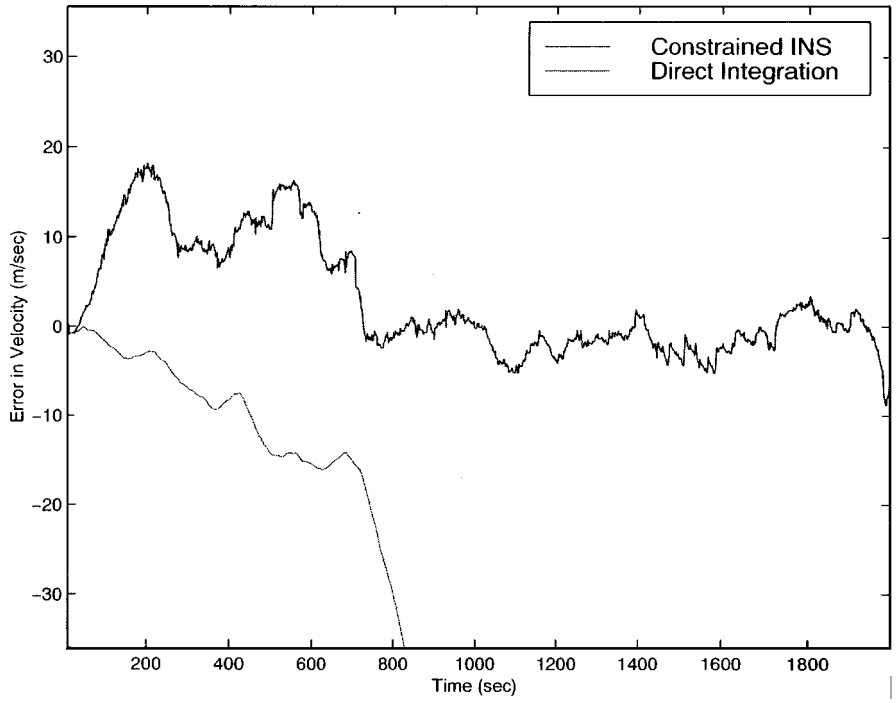

Fig. 3. Errors in vehicle speed when the vehicle is moving at a constant velocity of 10 m/s while the angular velocity about $\mathbf{b}_y$ is nonzero in the time interval 700–1300 s.

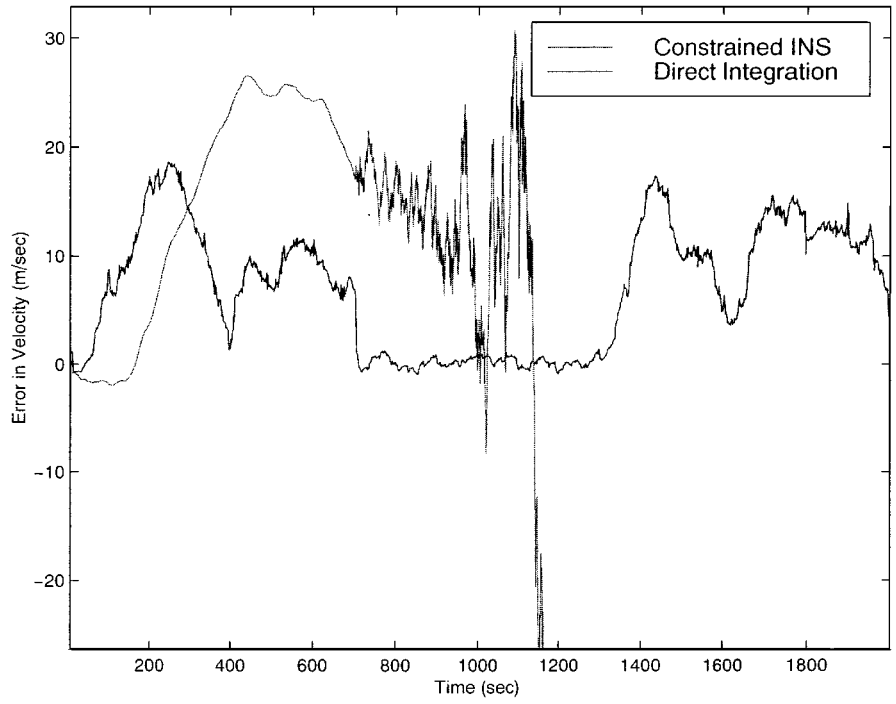

Fig. 4. Errors in vehicle speed when the vehicle is moving at a constant velocity of 10 m/s while the angular velocity about $\mathbf{b}_z$ is nonzero in the time interval 700–1300 s.

situations, firstly using the algorithm discussed in [11] for fusing information from IMU and GPS sensors, and secondly using the extended Kalman filter with constraints. The difference in position between these two methods is so small that it cannot be seen clearly in this plot. The "true" position and velocity of the vehicle that is used in subsequent results is obtained from the IMU/GPS algorithm.

Figs. 10 and 11 show the errors in position and velocity of the vehicle estimated using direct integration of the inertial data and using the constraint based filter. As shown, the position error increases quadratically such that after approximately 2 min (note that the axes are labeled in terms of inertial iteration counts), the free IMU result has drifted to over 750 m N, 300 m E, while the constrained based algorithm produces an error which stays

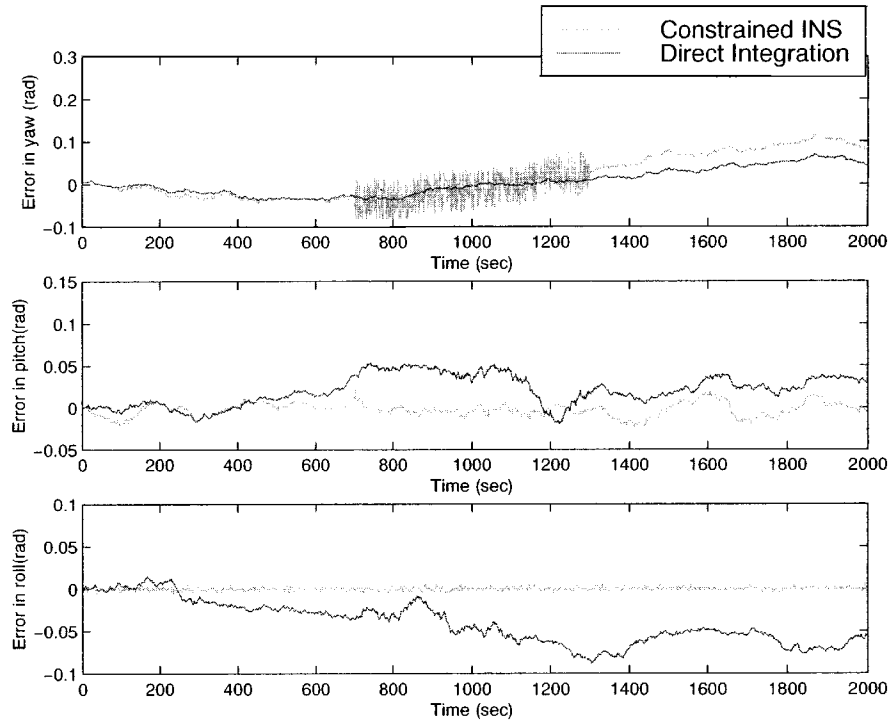

Fig. 5. Errors in roll, pitch, and yaw when the vehicle is moving at a constant velocity of 10 m/s while the angular velocity about $\mathbf{b}_z$ is nonzero in the time interval 700–1300 s.

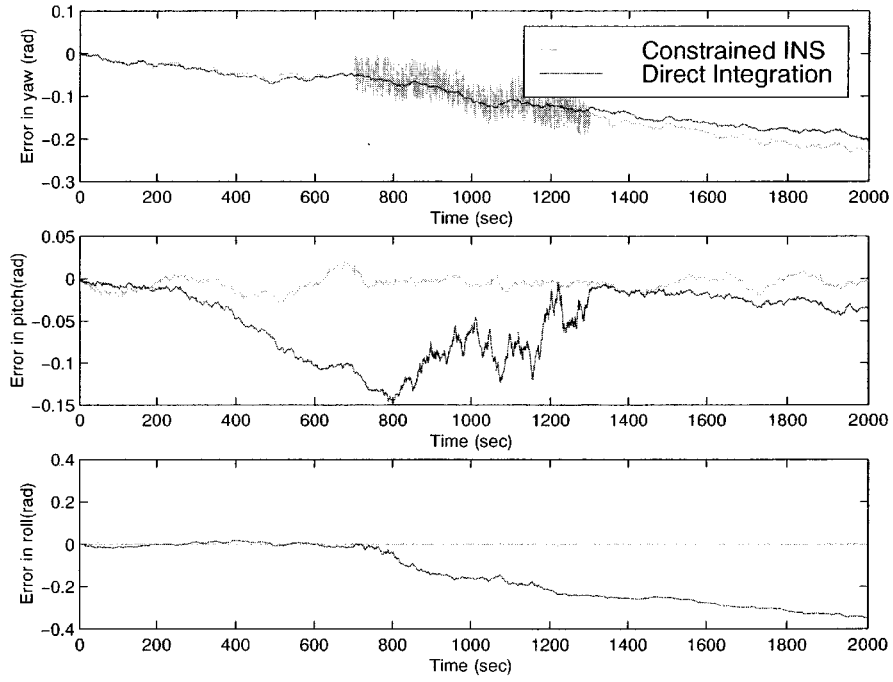

Fig. 6. Errors in roll, pitch, and yaw when the vehicle is moving at a constant velocity of 10 m/s while the angular velocity about $\mathbf{b}_z$ is nonzero in the time interval 700–1300 s. A constant unestimated bias of 10^{-4} rad/s is introduced to all angular velocity observations.

below 10 m N, 5 m E. Similarly, the velocity error increases linearly in the case of direct integration such that an error of approximately 10 m/s N, 5 m/s E is observed where as these errors are much smaller (less than 1 m/s) when the constraints are utilized.The path taken by the vehicle as estimated by the IMU/GPS system and the proposed algorithm. Figs. 12 and 13 show the errors in roll and pitch accumulated at the end of the trial run after the vehicle has stopped. When the vehicle is stationary the "true" roll and pitch can be obtained by two tilt sensors incorporated in the IMU, which have an accuracy of 0.1°. It is seen that the direct integration results in greater error than that of the constrained method. It is these roll and pitch errors that cause incorrect compensation for the gravitational acceleration, resulting in velocity errors and hence position drift.

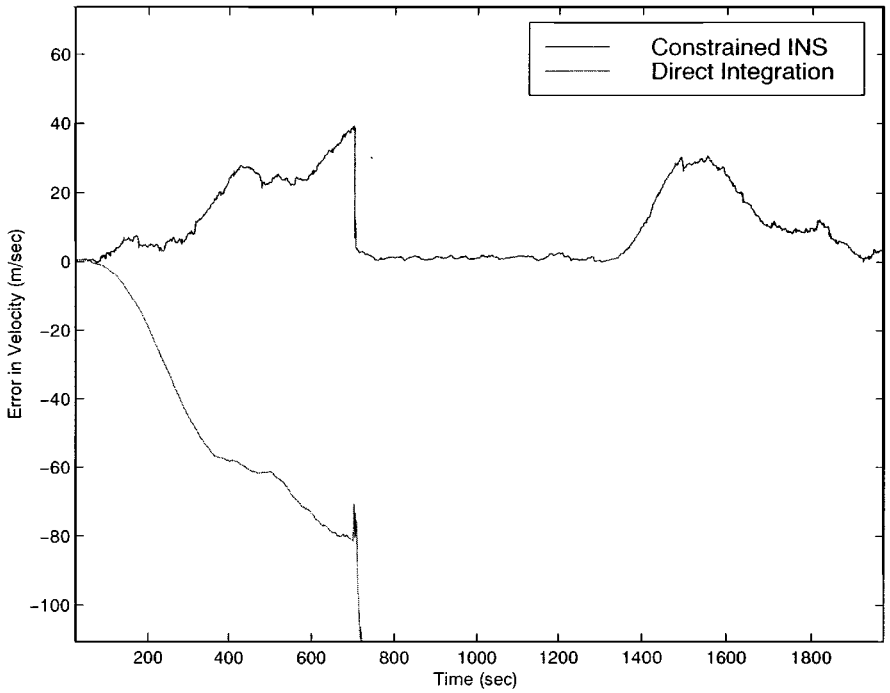

Fig. 7. Errors in the vehicle speed when the vehicle is moving at a constant acceleration of 0.05 m/s^2 for 1000 s and then decelerating at the same rate for another 1000 s. The angular velocity about $\mathbf{b}_z$ is nonzero in the time interval 700–1300 s.

Fig. 8. The vehicle used in the experiments. The IMU is placed in the rear tray. A differential RTK GPS unit is also present providing position and velocity of the vehicle to accuracies of 0.02 m and 0.02 m/s, respectively. The drive wheel encoder is located at the left rear wheel.

It is clear that the use of constraints in the computations significantly improves the location estimates obtained.

C. Experimental Results With an Aided IMU

Finally the results of a real time implementation of the inertial navigation system based on the linear information filter and the assumptions discussed in section Section III is presented. Note that the results presented here are of a much longer experiment than that presented in the previous section. The filter implemented uses constraints, encoder velocity and GPS information. The results are discussed into two parts; firstly only the information from the constraints and the speed sensor are utilized to demonstrate that the linearization assumptions are extremely satisfactory in practice, and secondly the complete information filter that also uses the GPS and the wheel encoder to show the effectiveness of the algorithm presented in Section III in a practical navigation system.

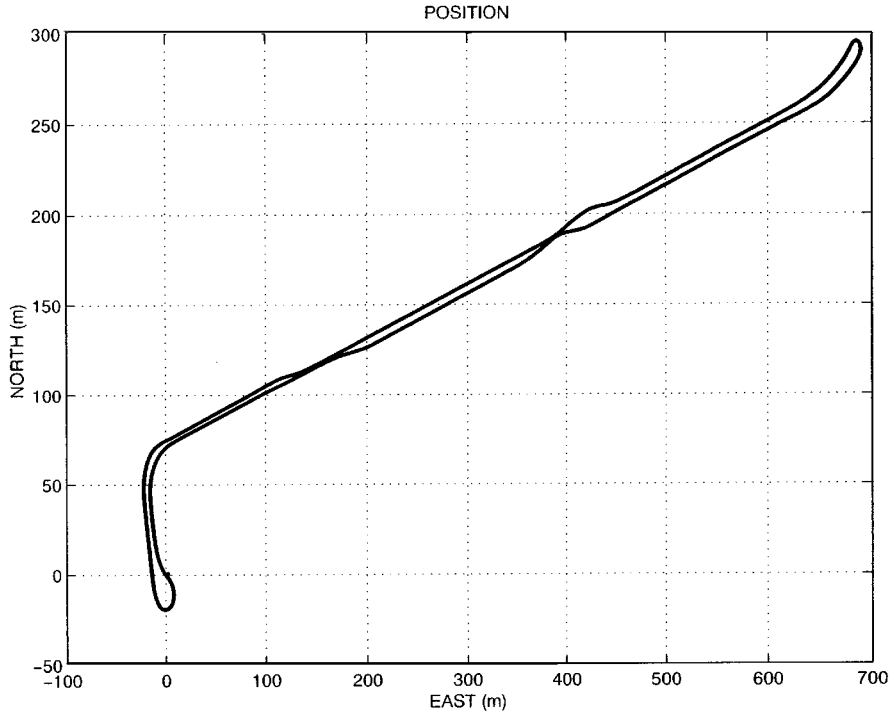

Fig. 9. The path taken by the vehicle as estimated by the IMU/GPS system and the proposed algorithm. The difference between the paths is too small to be seen clearly. The vehicle was driven at speeds of up to 10 m/s on a tarred road for about two minutes during this experiment.

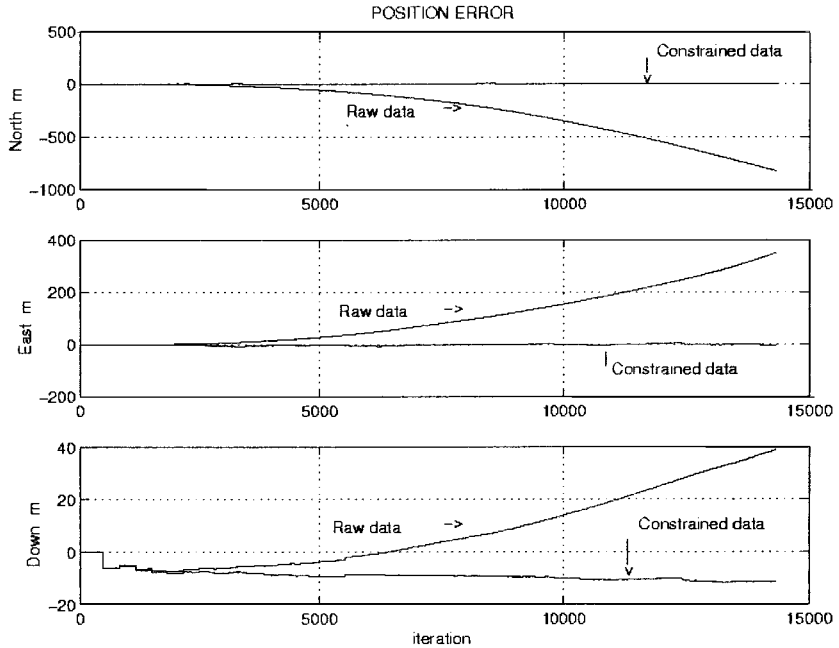

Fig. 10. Errors in position estimated using direct integration and the proposed constraint motion algorithm. The "true" position used to compute these errors was obtained using the IMU/GPS system.

Fig. 14 shows the position error in North and East directions when the inertial unit is used as a stand alone sensor, and when the vehicle speed and virtual observations due to constraints are used. As before results from the fusion of IMU/GPS based on [11] is used to provide the ground truth. As seen, the error growth of the position is bounded in this situation. Likewise Fig. 15 shows that the velocity error does not grow due to the use of these observations.

Fig. 16 shows the roll and pitch of the vehicle. As mentioned previously, any drift in these states causes the velocity, and hence position evaluation, to drift as well. Thus the addition of the virtual observation corrects the attitude and velocity of the inertial unit, thus minimizing the impact of drift on these states. Since the attitude is corrected, the velocity error of the unit is contained and hence position error minimized. It can be seen that the results are very similar to those obtained with the full nonlinear implementation.

With the addition of GPS observations, more information is provided to align the inertial system since this information can be inherently derived from the velocity obtained through the GPS.

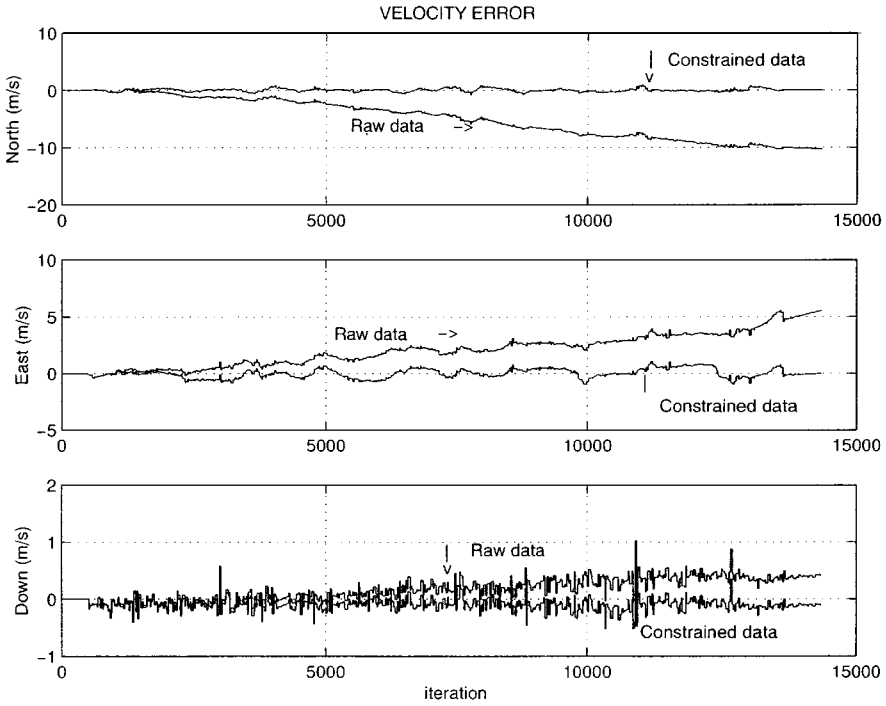

Fig. 11. Errors in velocity estimated using direct integration and the proposed constraint motion algorithm. The "true" velocity used to compute these errors was obtained using the IMU/GPS system.

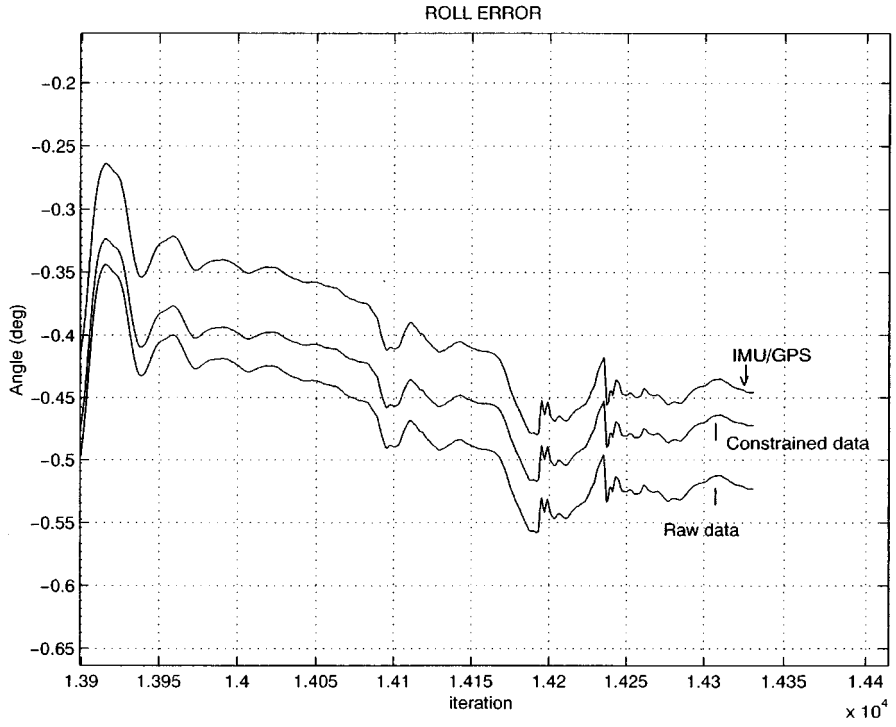

Fig. 12. Errors in roll accumulated at the end of the trial run (after about 2 mins), estimated using direct integration and the proposed constraint motion algorithm. The error in the IMU/GPS solution is provided as well. The "true" roll angle is provided by tilt sensors which have an accuracy of 0.1° when the vehicle is stationary.

The position observations from the GPS avoids the lack of observability encountered with the constraint only implementation. The greater the frequency of observations from the GPS unit, the more information is added to the estimate [see (33) and (34)].

Figs. 17–19 compare the constrained inertial unit and the constrained inertial unit with GPS observations provided every 15 s. When comparing the plots, the greatest improvement can be seen with the position error since this is unobservable with the use of constraints alone. Improvements in the estimated velocity and attitude of the inertial system can also be seen. However, these improvements are minimal since the states are already observable even when the virtual observations

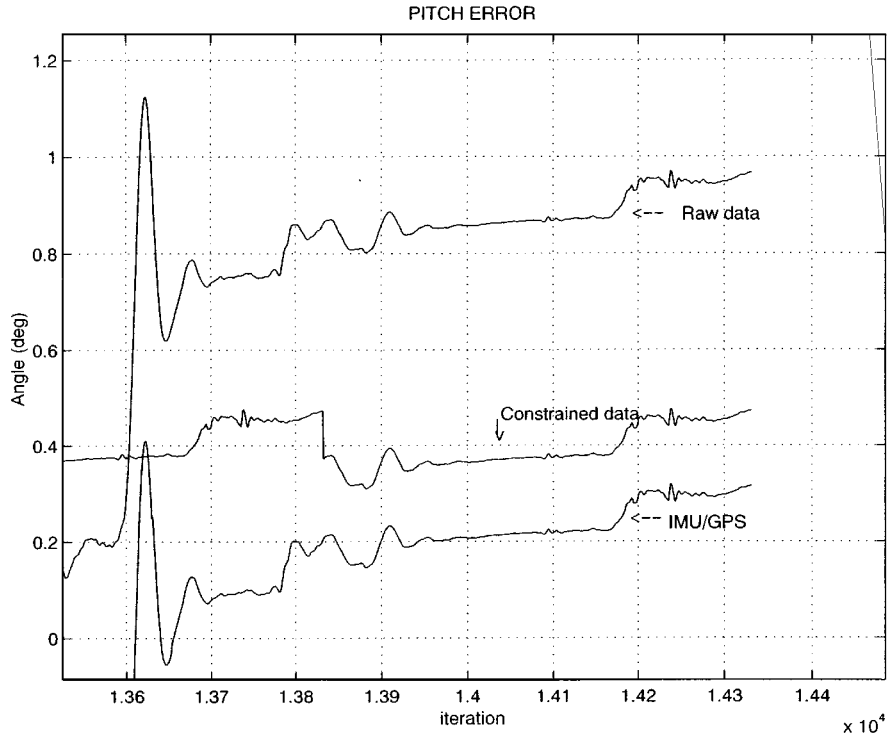

Fig. 13. Errors in pitch accumulated at the end of the trial run (after about 2 min), estimated using direct integration and the proposed constraint motion algorithm. The error in the IMU/GPS solution is provided as well. The "true" pitch angle is provided by tilt sensors which have an accuracy of 0.1° when the vehicle is stationary.

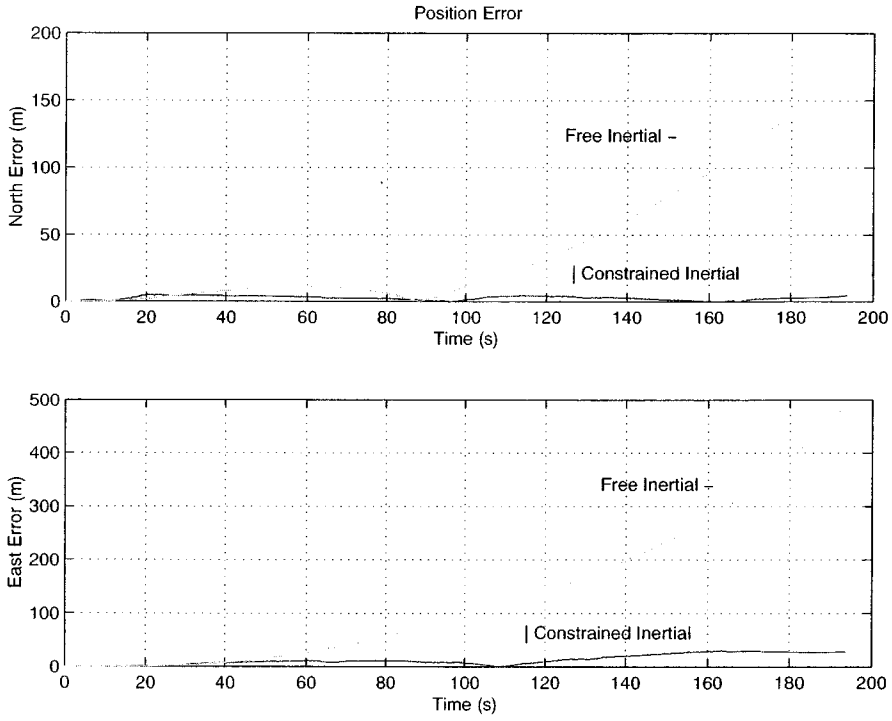

Fig. 14. Errors in position estimated using direct integration and the proposed constraint motion algorithm based on the linear information filter. The "true" position used to compute these errors was obtained using the IMU/GPS system.

due to constraints are used. Furthermore, the latter provides a significant amount of information due to the high update rate used in the application of constraints. The more frequently the GPS observations are added, the less error will develop in the attitude and velocity of the inertial system. More importantly however, these results show that the errors in the estimates obtained using only inertial data can be contained between GPS fixes. This dramatically improves the navigation suite as a whole, since the inertial system can navigate for a substantially greater amount time without GPS. The duration of this time is in turn dependent on the accuracy of the inertial unit used and the target application.

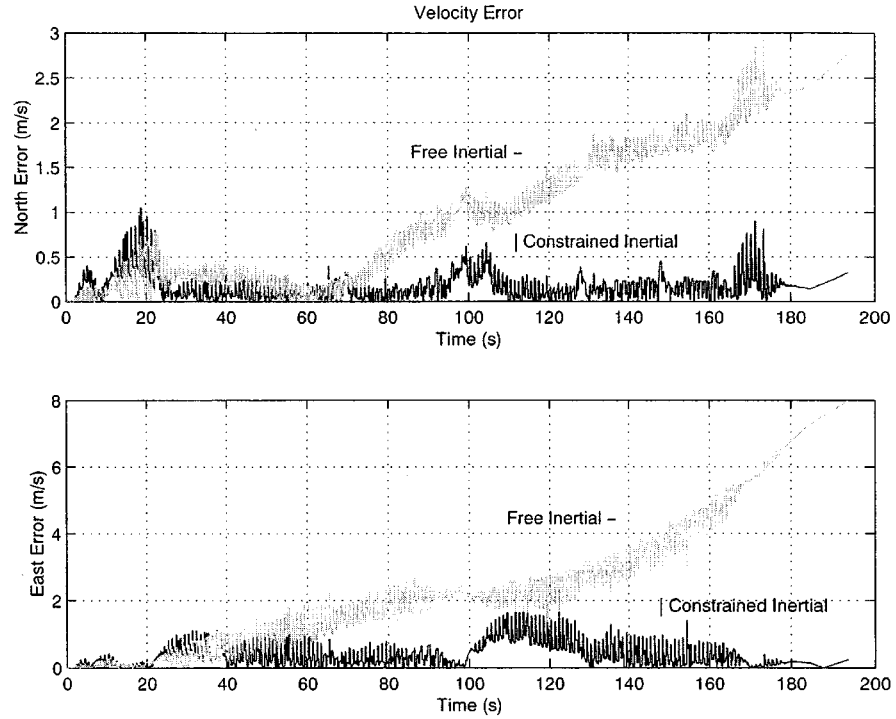

Fig. 15. Errors in velocity estimated using direct integration and the proposed constraint motion algorithm based on the linear information filter. The "true" velocity used to compute these errors was obtained using the IMU/GPS system.

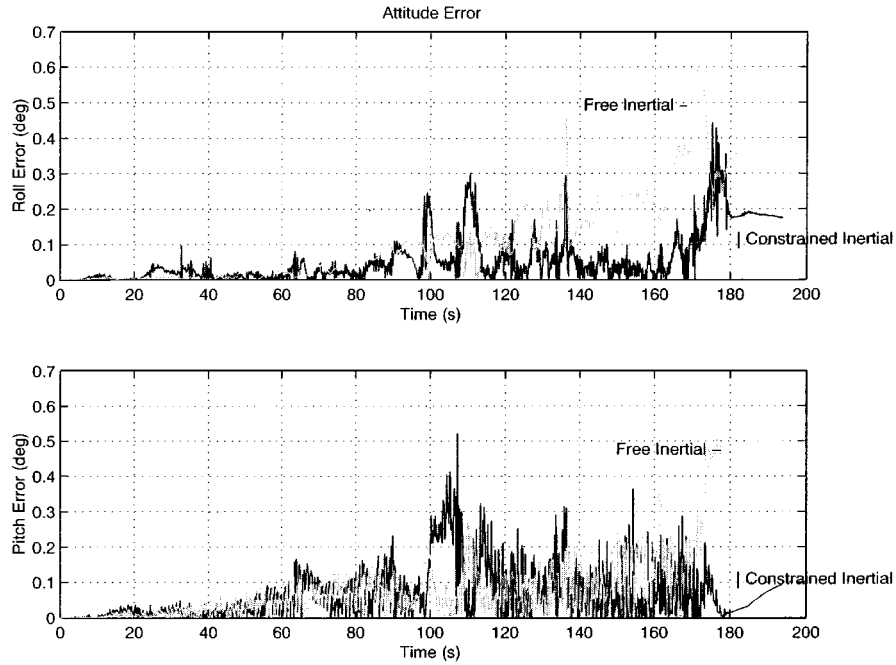

Fig. 16. These two plots show the roll and pitch errors accumulated at the end of the trial run, obtained using direct integration and the proposed constraint motion algorithm based on the linear information filter. The "true" attitude angles were provided by tilt sensors which have an accuracy of 0.1° when the vehicle is stationary.

D. Summary of Results

Tables I and II provide a summary of the experimental results obtained.

V. Conclusion

The popularity of IMUs in the automotive industry is ever increasing. The major disadvantage of using a low-cost strapdown inertial system is the rapid error growth that is encountered. This is primarily due to drift in attitude estimate of the unit caused by the noise and nonlinearities in the gyro data. With the algorithm presented in this paper, the duration of time for which an IMU can be relied upon as the sole navigation tool can be significantly extended as compared to conventional techniques.

The core of the algorithm presented lies in the use of constraints that govern the motion of the vehicle. It was shown that

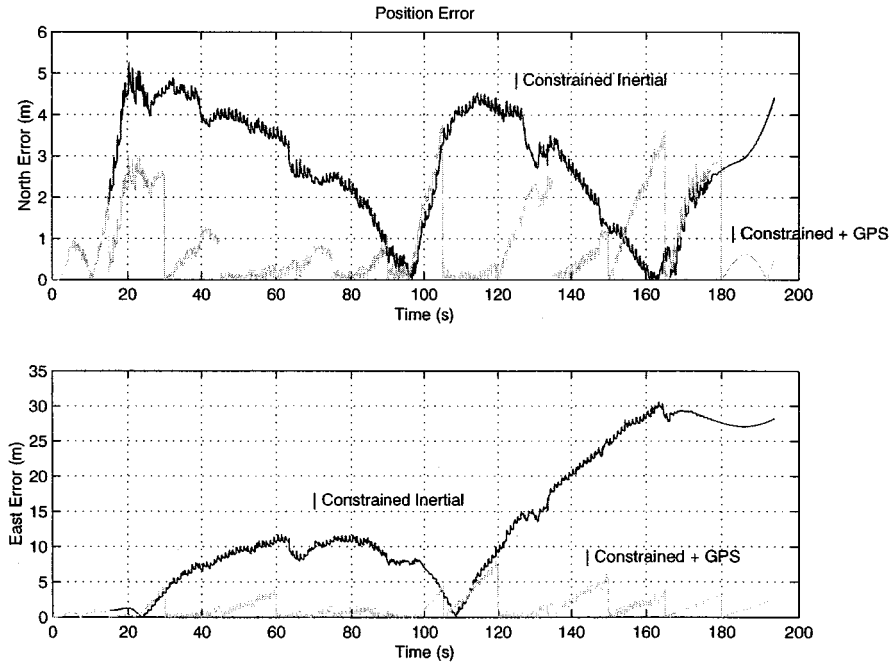

Fig. 17. These two plots show the error in position obtained with the virtual velocity observation, and with the virtual velocity and GPS every 15 s. Even at this low sampling rate, incorporation of the information from GPS dramatically improves the resulting position estimates.

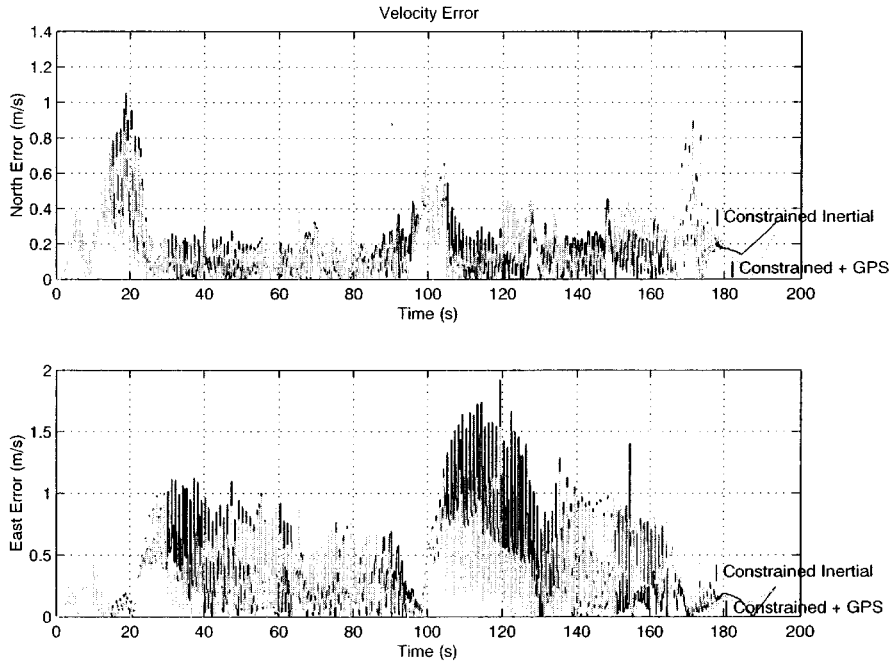

Fig. 18. These two plots show the error in velocity obtained with the virtual velocity observation, and with the virtual velocity and GPS every 15 s. As velocity is observable between the GPS fixes, the improvement obtained is only marginal.

under ideal conditions the velocity of the vehicle in the body frame is represented by a vector in the forward direction, that is, along the x axis. Hence the velocity along the remaining two axes, namely y and z, are constrained to be zero. However, due to the presence of wheel slip and the effects of the suspension commonly encountered in land vehicles, the velocities in these two directions are not identically zero. As a first approximation, these velocities were simply modeled as white noise. This appears satisfactory in many situations and the experimental results show a dramatic improvement in the position estimates obtained. Slip or vibrations cannot be regarded insignificant in all land vehicles, in particular for vehicles that operate in rough terrain. These effects, therefore, need to be modeled appropriately if the use of white noise is not a sufficiently accurate representation.

The information filter framework has allowed for the addition of multiple observations to aid the inertial unit. The implementation described in this work can be further extended to include attitude provided by either GPS or tilt sensors. Most importantly, the addition of the observations due to the constraints bounds the

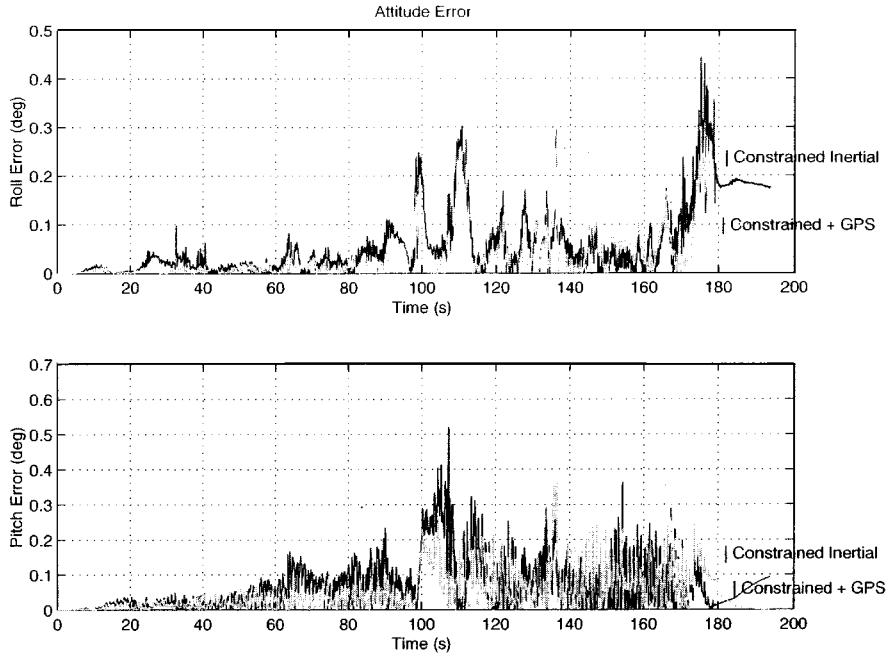

Fig. 19. Error in attitude obtained with the virtual velocity observation, and with the virtual velocity and GPS every 15 s. As in the previous case of velocity, only a slight improvement is seen when the GPS observations are used. This again is due to the fact that the attitude is observable between GPS fixes. The jump in the pitch error seen at the end of the run is due to a jump in velocity fix from the GPS receiver.

TABLE I
SUMMARY OF RESULTS FOR THE FIRST EXPERIMENT. COMPARISON OF THE FREE INERTIAL SOLUTIONS TO THE AIDED INERTIAL SOLUTIONS USING THE CONSTRAINT OBSERVATIONS

Method implemented (2mins)	Position Error (m)	Velocity Error (m/s)	Attitude Error (°)
Free Inertial	750N 300E	10N 5E	0.53 Roll 0.96 Pitch
Constrained Inertial	10N 5E	< 1 N,E	0.41 Roll 0.45 Pitch

TABLE II
SUMMARY OF RESULTS FOR THE SECOND EXPERIMENT. COMPARISON OF THE FREE INERTIAL SOLUTIONS TO THE AIDED INERTIAL SOLUTIONS USING THE CONSTRAINT OBSERVATIONS AND SPEED DATA IN THE INFORMATION FILTER, AND CONSTRAINT OBSERVATIONS, SPEED DATA AND GPS IN THE INFORMATION FILTER. THE JUMP IN THE PITCH ESTIMATION WHEN USING GPS IS DUE TO A JUMP IN THE VELOCITY FIX FROM THE GPS RECEIVER

Method implemented (3.5mins)	Position Error (m)	Velocity Error (m/s)	Attitude Error (°)
Free Inertial	140N 400E	2.5N 7E	0.35 Roll 0.5 Pitch
Constrained/Speed Inertial	4N 26E	0.25N 0.25E	0.18 Roll 0.05 Pitch
Constrained/Speed/GPS Inertial	0.5N 0.15E	0.23N 0.25E	0.15 Roll 0.07 Pitch

error growth of the attitude and velocity of the inertial system thus also bounding the position errors. This has a dual effect of providing more information to aid the IMU when GPS observations are obtained, and furthermore contains the error growth between GPS observations, which is highly desirable in situations where GPS signal outages or multipath can occur.

VI. FURTHER WORK

There are principally two areas where this algorithm can be further developed. The first is the modeling of the constraints using the knowledge of the vehicle to ground interactions. This will then cover a wider range of land vehicles and also provide a better representation of the constraints. The second area is the investigation of the minimum number of inertial sensors required to predict the position of a land vehicle considering the nonholonomic constraints. This is of fundamental importance since this in turn will reduce the cost of inertial systems used on land vehicles.

REFERENCES

[1] S. Scheding, G. Dissanayake, E. Nebot, and H. Durrant-Whyte, "An experiment in autonomous navigation of an underground mining vehicle," *IEEE Trans. Robot. Automat.*, vol. 15, pp. 85–95, Feb. 1999.
[2] F. Van Diggelen, "GPS and GPS + GLONASS RTK," in *ION-GPS*, Sep 1997.
[3] M. Ollis and A. Stentz, "Vision-based perception for an autonomous harvester," in *Proc. IEEE/RSJ Int. Conf. Intelligent Robotic Systems*, Sept. 1997, pp. 1838–1844.
[4] S. Sukkarieh, E. M. Nebot, and H. Durrant-Whyte, "Achieving integrity in an ins/gps navigation loop for autonomous land vehicle applications," in *IEEE Int. Conf. Robotics and Automation*, May 1998, pp. 3437–3442.
[5] E. Nebot and H. Durrant-Whyte, "A high integrity navigation architecture for outdoor autonomous vehicles," *Robot. Auton. Syst.*, vol. 26, pp. 81–97, February 1999.
[6] E. Krotkov and F. Fuke, "Dead reckoning for lunar rover in uneven terrain," in *IEEE Int. Conf. Robotics and Automation*, 1997, pp. 411–416.
[7] C. H. J. Fox and D. J. W. Hardie, "Vibratory gyroscopic sensors," in *Symp. Gyro Technology*, 1995.
[8] B. Salaberry, "A low cost vibrating gyro for guidance applications and automotive application," in *Symp. Gyro Technology*, 1998.

[9] G. Fetzer, W. Golderer, and J. Gerstenmeier, "Yaw rate sensor in silicon micromachining technology for automotive applications," in *Symp. Gyro Technology*, 1998.
[10] R. Hulsing, "MEMS inertial rate and acceleration sensor," in *IEEE Position, Location and Navigation Symp.*, 1998, pp. 17–23.
[11] S. Sukkarieh, E. M. Nebot, and H. Durrant-Whyte, "A high integrity IMU/GPS navigation loop for autonomous land vehicle applications," *IEEE Trans. Robot. Automat.*, vol. 15, pp. 572–578, June 1999.
[12] ——, "The GPS aiding of INS for land vehicle navigation," in *FSR97 Field Service Robotics*. Berlin, Germany: Springer-Verlag, 1998, pp. 267–274.
[13] M. Koifman and Y. Bar-Itzhack, "Inertial navigation system aided by aircraft dynamics," *IEEE Contr. Syst. Technol.*, vol. 7, pp. 487–497, July 1999.
[14] P. Maybeck, *Stochastic Models, Estimation and Control*. New York: Academic, 1982, vol. 1.
[15] Y. Bar-Shalom and X. Li, *Estimation and Tracking —Principles, Techniques and Software*. Norwell, MA: Artech House, 1993.
[16] P. Maybeck, *Stochastic Models, Estimation and Control*. New York: Academic, 1982, vol. 2.
[17] S. Sukkarieh, "Aided Inertial Navigation Systems for Autonomous Vehicles,", University of Sydney, 2000.

Gamini Dissanayake graduated with a degree in mechanical/production engineering from the University of Peradeniya, Sri Lanka. He received the M.Sc. degree in machine tool technology and the Ph.D. degree in mechanical engineering (robotics) from the University of Birmingham, U.K., in 1981 and 1985, respectively.

He was a Lecturer at the University of Peradeniya and the National University of Singapore before joining the University of Sydney, Australia, where he is currently a Senior Lecturer attached to the Australian Centre for Field Robotics. His current research interests are in the areas of localization and map building for mobile robots, navigation systems, dynamics and control of mechanical systems, cargo handling, optimization, and path planning.

Salah Sukkarieh (S'97–A'00) received a degree in mechanical (mechatronics) engineering and received the Ph.D. degree from the University of Sydney, Australia.

He became a faculty member in 2001 and is affiliated with the Australian Centre for Field Robotics. His current research activities include INS/GPS integration, decentralised navigation and control algorithms.

Eduardo Nebot (S'79–M'81) received the B.S. degree in electrical engineering from the Universidad Nacional del Sur, Argentina, and the M.S. and Ph.D. degrees from Colorado State University, Fort Collins.

He is Associate Professor at the University of Sydney, Australia, in the Department of Mechanical and Mechatronic Engineering, where he has been a faculty member since 1992. His current research contents Inertial sensors, GPS and inertial sensing in land vehicle applications, navigation and guidance algorithms; decentralized and distributed navigation, map-building, and terrain-aiding. He has also been involved in different automation projects in the stevedoring, mining and cargo handling industries. He is currently the Automation Program manager for the Centre for Mining, Technology and Equipment.

Hugh Durrant-Whyte, photograph and biography not available at the time of publication.